


## Phase behavior of active and passive dumbbells

Nayana Venkatareddy <sup>1</sup>, Shiang-Tai Lin <sup>2</sup>, and Prabal K. Maiti <sup>1,\*</sup>

<sup>1</sup>*Department of Physics, Indian Institute of Science, C. V. Raman Ave, Bengaluru 560012, India*

<sup>2</sup>*Department of Chemical Engineering, National Taiwan University, Taipei, Taiwan 10617*

 (Received 11 August 2022; revised 5 February 2023; accepted 8 March 2023; published 29 March 2023)

We report phase separation in a mixture of “hot” and “cold” three-dimensional dumbbells which interact by Lennard-Jones potential. We also have studied the effect of asymmetry of dumbbells and the variation of ratio of “hot” and “cold” dumbbells on their phase separation. The ratio of the temperature difference between hot and cold dumbbells to the temperature of cold dumbbells is a measure of the activity  $\chi$  of the system. From constant density simulations of symmetric dumbbells, we observe that the “hot” and “cold” dumbbells phase separate at higher activity ratio ( $\chi > 5.80$ ) compared to that of a mixture of hot and cold Lennard-Jones monomers ( $\chi > 3.44$ ). We find that, in the phase-separated system, the hot dumbbells have high effective volume and hence high entropy which is calculated by two-phase thermodynamic method. The high kinetic pressure of hot dumbbells forces the cold dumbbells to form dense clusters such that at the interface the high kinetic pressure of hot dumbbells is balanced by the virial pressure of cold dumbbells. We find that phase separation pushes the cluster of cold dumbbells to have solidlike ordering. Bond orientation order parameters reveal that the cold dumbbells form solidlike ordering consisting of predominantly face-centered cubic and hexagonal-close packing packing, but the individual dumbbells have random orientations. The simulation of the nonequilibrium system of symmetric dumbbells at different ratios of number of hot dumbbells to cold dumbbells reveals that the critical activity of phase separation decreases with increase in fraction of hot dumbbells. The simulation of equal mixture of hot and cold asymmetric dumbbells revealed that the critical activity of phase separation was independent of the asymmetry of dumbbells. We also observed that the clusters of cold asymmetric dumbbells showed both crystalline and noncrystalline order depending on the asymmetry of dumbbells.

DOI: [10.1103/PhysRevE.107.034607](https://doi.org/10.1103/PhysRevE.107.034607)

### I. INTRODUCTION

Active matter consists of individual units which are driven out of equilibrium as they consume energy from the surrounding medium or through internal mechanisms. Examples of active matter are present in all length scales from the sub-cellular cytoskeleton [1–6], bacterial colonies, and collection of cells in a tissue [7–10] to collection of organisms like swarms of fish, flocks of birds [11–19], etc. Active matter like Janus particles [20,21] can also be artificially synthesized and has wide application in medicine like drug delivery [22] and nanomachines [23]. They exhibit fascinating properties like phase separation and self-organization [24–50] and play very important role in biological systems.

In many studies on active particles, the activity of the constituents is represented by a vector model. In vector models like active Brownian particles [51,52] and run and tumble particles [53,54], the constituent particle (e.g., bacteria) absorbs energy to generate a force which propels it in a particular direction (usually along the body axis). The activity is a measure of how much energy the constituent particle can take and convert into work (live bacteria have high activity but dead bacteria have zero activity). Recent studies have shown that for a system of mixture of passive and active particles (run

and tumble particles), in the limit when persistence length (length traveled with constant swim speed by the particle before changing direction) of active particles is comparable to the radius of the particle, the system of active and passive particle reduces to that of a system of “hot” and “cold” particles [55]. Also many active matter systems have been characterized with an effective temperature [56–58] replacing the temperature of medium in the fluctuation-dissipation theorem. The effective temperature of the active particles is much greater than the medium temperature and is proportional to the magnitude of active forces. Such representation of vectorial activity by different temperatures reduces a vector model into scalar model. Theoretical works have explored the rich phase behavior shown by mixture of particles connected to thermostats at different temperatures [59,60]. In a scalar model, the activity differences between two species in a system (e.g., live and dead) is represented by assigning two different temperatures or two different diffusivities [61,62] to two species. For example, Ganai *et al.* [63] have proposed the use of a scalar model to explain the radial distribution of chromatin inside nucleus. Phase separation in a system of equal mixture of hot and cold Lennard-Jones (LJ) particles at different densities has been studied [64]. Recently, we have done simulation in a two-temperature model of soft repulsive spherocylinders and have shown emergence of various liquid crystalline order at packing fractions for which only isotropic phase is possible in equilibrium [65–67].

\*maiti@iisc.ac.in

In this paper, we study phase separation in system of hot and cold dumbbells [68] which interact by LJ potential. Dumbbells are not only a simplest way to model anisotropic particles but they also show interesting crystal structures in equilibrium. In equilibrium, the dumbbells with low aspect ratio form plastic crystals with no orientational ordering [69] while the dumbbells with high aspect ratio form crystals with both translational and orientational order. Also, asymmetric dumbbells [70,71] show rich phase behavior by forming rotator, NaCl,  $\alpha$ IrV, CrB, and  $\gamma$ CuTi equivalent crystal structures. In some recent works, colloidal dumbbells have been used to build periodic crystal structures which have partial photonic bandgap and are birefringent [72]. Also, there are experimental works that have built chiral colloidal structures [73] with asymmetric dumbbells [71,74] using magnetic fields. So the dumbbells have garnered much interest in nanotechnology of colloids. Also, there has been increased interest in active dumbbells, as some computational studies [56,75,76] on two-dimensional active dumbbells described by vector model showed phase separation of active dumbbells into a dilute phase and dense phase with hexatic order and interesting polarization and velocity field. Recently, experiments on active dumbbells which propel on exposure to light have again confirmed that the active dumbbells phase separate into a dilute phase and dense swimmer phase [77]. They also observed that when active dumbbells were mixed with passive particles, the active dumbbells corral the passive particles.

We have used scalar model of activity to study the phase behavior of active and passive dumbbells where active dumbbells are connected to a thermostat at high temperature and passive dumbbells are connected to a thermostat at low temperature. The ratio of the temperature difference between hot and cold dumbbells to the temperature of cold dumbbells is defined as the activity  $\chi$  of the nonequilibrium system. The system shows phase separation at sufficiently high activity.

The paper is organized as follows: In the next section, we give details of the simulation methodology. In Sec. III, we present results for both the passive and active system. We discuss the equilibrium properties of the symmetric dumbbells including the entropy calculation using both thermodynamic perturbation and two-phase thermodynamic (2PT) method. This is followed by the discussion of the results for nonequilibrium system of equal mixture of hot and cold symmetric dumbbells in Sec. III B. Our simulations demonstrate that the mixture of hot and cold dumbbells phase separate at all densities for sufficiently high activity, although the extent of phase separation decreases with density. We also find that the critical activity (activity at which phase separation becomes macroscopic) of dumbbells ( $\chi > 5.80$ ) is greater than the critical activity of LJ monomers ( $\chi > 3.44$ ). In our system, activity is introduced by raising the temperature of hot dumbbells relative to cold dumbbells. So to determine the effect of activity on hot dumbbells in the nonequilibrium system with respect to their corresponding equilibrium counterparts, we calculate entropy difference  $\Delta S$  between hot dumbbells of nonequilibrium system ( $S^{\text{neq}}$ ) and entropy of corresponding equilibrium system ( $S^{\text{eq}}$ ). We find that the entropy difference  $\Delta S$  jumps from negative to positive value with the onset of phase separation. Further, on performing cluster analysis of cold dumbbells, we find that with increasing activity  $\chi$  the

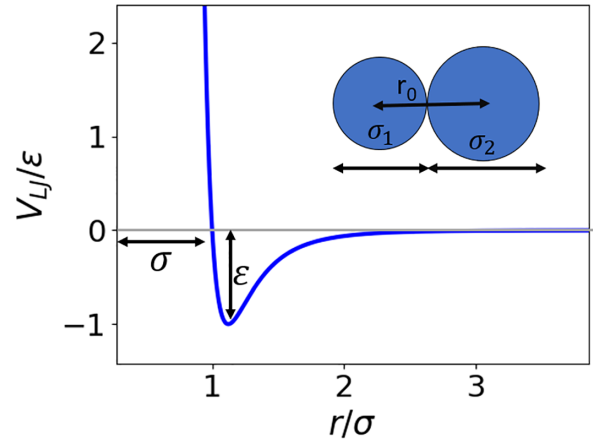


FIG. 1. The plot of Lennard-Jones potential with which the dumbbells interact. In the inset, schematic diagram of a dumbbell is shown. Two atoms of different diameters  $\sigma_1$  and  $\sigma_2$  are bonded to form a dumbbell.  $r_0$  is the distance between centers of two atoms in a dumbbell.

number of cluster of cold dumbbells decrease, while the size of largest cluster increases. The packing fraction, temperature, and pressure variation along the length of the simulation volume reveal that high kinetic pressure of the hot dumbbells force the cold dumbbells to form dense clusters whose viral pressure balances the kinetic pressure of hot dumbbells. Bond orientation order parameters are calculated which reveal that the cold cluster develops solidlike order with predominantly face-centered cubic (fcc) and hexagonal-close packing (hcp) arrangement. In Sec. III C, we discuss the results of simulation of the nonequilibrium system at different mixing ratios of hot and cold dumbbells. We find that critical activity decreases with the increase in fraction of hot dumbbells. Finally, in Sec. III D, we report the results of simulation of equal mixture of hot and cold dumbbells with different asymmetry. We find that their critical activity for phase separation is independent of asymmetry. We observe both crystalline and noncrystalline structures in cold clusters depending on the asymmetry.

## II. METHODOLOGY AND COMPUTATIONAL DETAILS

We start with a system of 8000 atoms where two atoms are bonded to form 4000 dumbbells. Each dumbbell has two atoms with diameter  $\sigma_1$  and  $\sigma_2$ . We define the asymmetry parameter  $\alpha = \frac{\sigma_1}{\sigma_2}$  as the ratio of the diameter of smaller atom to the diameter of the larger atom in a dumbbell. Interaction between atoms of the dumbbells of type  $i$  and type  $j$  is described by Lennard-Jones potential,

$$V_{\text{int}}(r) = 4\epsilon \left[ \left( \frac{\sigma_{ij}}{r} \right)^{12} - \left( \frac{\sigma_{ij}}{r} \right)^6 \right], \quad (1)$$

where  $r$  denotes the distance of separation between any two atoms and  $\epsilon$  correspond to the strength of the interaction potential of the atoms. A plot of LJ potential and schematic diagram of the dumbbell is shown in Fig. 1. Here we choose  $\sigma_{ij} = \frac{1}{2}(\sigma_i + \sigma_j)$  to be the arithmetic mean of the diameters of the two interacting atoms. In our simulation we have used  $\sigma_{11} = \alpha\sigma$ ,  $\sigma_{22} = \sigma$ , and  $\sigma_{12} = \frac{1}{2}(\sigma_1 + \sigma_2)$ . We have used the

parameters of argon ( $\sigma = 3.405 \text{ \AA}$ ,  $\epsilon = 0.238 \text{ kcal mol}^{-1}$ , and mass  $m = 39.948 \text{ g mol}^{-1}$ ) to convert the LJ units to real units. Two atoms within a dumbbell are held by a harmonic bond potential of the following form:

$$V_{\text{bond}}(r) = k(r - r_0)^2, \quad (2)$$

where  $r_0$  is the equilibrium bond length and  $k$  is bond strength. In our simulations, we have taken  $r_0 = \frac{1}{2}(\sigma_1 + \sigma_2)$  to be arithmetic mean of the diameters of two atoms in dumbbell and  $k$  equal to  $3000\epsilon/\sigma^2$  as per the original LJ chain paper [78]. For symmetric dumbbell, asymmetry parameter  $\alpha = 1$  and  $\sigma_{11} = \sigma_{22} = \sigma_{12} = \sigma$ .

The Nosé-Hoover thermostat with damping parameter  $50\delta t$  is used to maintain the temperature of the dumbbells in the NVT ensemble. The time step of integration was chosen to be  $\delta t = 1 \text{ fs}$  for all the simulations reported in this work. All the simulations are performed using the LAMMPS [79] molecular dynamics package.

### III. RESULTS AND DISCUSSION

#### A. Equilibrium properties of symmetric dumbbells

In order to validate our system of symmetric dumbbells ( $\alpha = 1$ ), we first calculate the equation of state and entropy of symmetric dumbbells. The temperature  $T^*(k_b T/\epsilon)$  and pressure  $P^*(P\sigma^3/\epsilon)$  are in reduced units. We run the MD simulation of dumbbells in the NVT ensemble at  $T^* = 3, 4, 5$  (LJ units) at different packing fractions  $\eta$  ( $\eta = \frac{Nv_0}{V}$ , where  $N$  is the number of dumbbells in simulation box with volume  $V$  and  $v_0$  is the volume of individual dumbbell) to obtain the pressure of the system. The pressure obtained from simulation is compared with pressure obtained from Wertheim's thermodynamic perturbation theory [78,80]. According to the thermodynamic perturbation theory, the excess Helmholtz free energy of Lennard-Jones chain can be obtained from excess Helmholtz free energy of Lennard-Jones monomer fluid as follows:

$$\frac{A_e^n(\rho_n)}{N} = \frac{A_e(\rho)}{N} + T \frac{1-n}{n} \ln y(\sigma), \quad (3)$$

Here  $A_e^n$  is the excess free energy of LJ chain composed of  $n$  monomers (for dumbbells  $n = 2$ ),  $A_e$  is the excess free energy of Lennard-Jones monomer fluid,  $N$  is the total number of monomers,  $\rho$  is the monomer number density, and  $y(\sigma)$  is the pair correlation function of LJ monomer fluid at distance equal to bond length  $\sigma$  (since we are interested about dumbbells whose bond length is  $\sigma$ , we consider the value of pair correlation function of LJ monomers at distance  $\sigma$ ). Differentiating Eq. (3) with respect to density we obtain the expression for pressure,

$$P^n(\rho_n) = P(\rho) + \rho T \frac{1-n}{n} \left[ 1 + \rho \frac{\delta \ln y(\sigma)}{\delta \rho} \right]. \quad (4)$$

Here  $P^n$  is pressure of LJ chain fluid and  $P$  is the pressure of LJ monomer fluid. The pair correlation function  $y(\sigma)$  of LJ monomers is obtained as an empirical fitting function where it is expressed in powers of density and temperature. The empirical form of the pair correlation  $y(\sigma)$  is obtained from the work of Gubbin's *et al.* [78]. Pressure of the fluid of LJ monomers  $P$  is obtained from MD simulations. Pressure

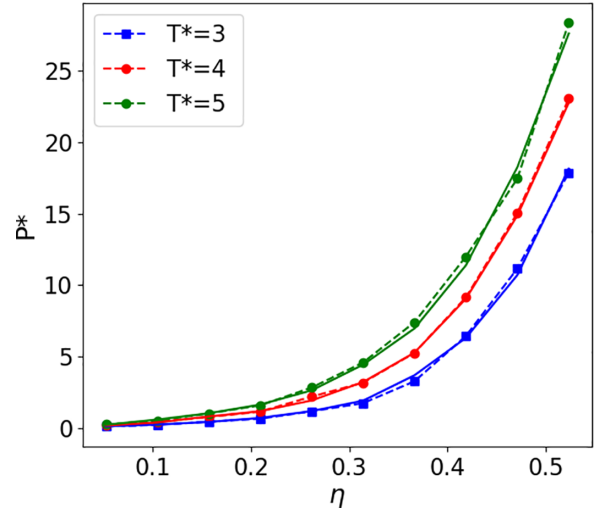


FIG. 2. Pressure of dumbbells  $P^*$  as a function of packing fraction  $\eta$  at temperature  $T^* = 3, 4$ , and  $5$ . Dashed lines represent pressure obtained from perturbation theory. The solid lines represent the pressure obtained from MD simulations.

obtained using Eq. (4) (dashed lines) is plotted as a function of density in Fig. 2. We can see that the pressure of dumbbells calculated from MD simulation (solid lines) matches closely with the values predicted by perturbation theory (dashed lines).

Next, we compute the entropy of symmetric dumbbells. Differentiating Eq. (3) with respect to temperature gives the expression for entropy as follows:

$$\frac{S_e^n(\rho_n)}{N} = \frac{S_e(\rho)}{N} + \frac{n-1}{n} \left[ \ln y(\sigma) + T \frac{\delta \ln y(\sigma)}{\delta T} \right], \quad (5)$$

where  $S_e^n$  is the excess entropy of LJ chain and  $S_e$  is excess free energy of LJ monomer fluid. The excess entropy of LJ monomer fluid  $S_e$  is obtained from the modified Benedict-Webb-Rubin equation of state [82]. To calculate the total entropy (excess entropy+ideal gas entropy)  $S$  of symmetric dumbbells from excess entropy of Lennard-Jones chain  $S_e^n$ , we consider two references. The excess entropy of Lennard-Jones chain  $S_e^n$  is calculated with respect to ideal monoatomic gas (TP1) which is plotted in green dashed lines and with respect to ideal diatomic gas (rigid rotor) (TP2) which is plotted in black dotted lines in Fig. 3.

The entropy  $S$  of dumbbells is also calculated using the 2PT method [83–85]. In the 2PT method, the first vibrational density of states of fluid is obtained from Fourier transform of velocity autocorrelation function. Then the vibrational density of states of the fluid is partitioned into a gas- and solidlike component. The gaslike component is treated as a hard sphere gas while the solidlike component is treated as harmonic oscillator. This decomposition into solid- and gaslike fractions is performed from the value of vibrational density of states of the liquid at zero frequency. Once the decomposition is done, by using the weighting functions of harmonic oscillator and hard sphere gas, various thermodynamic properties like entropy and free energy can be calculated. The entropy of dumbbell obtained from the 2PT method as a function of packing fraction is plotted in Fig. 3 (red dashed line).



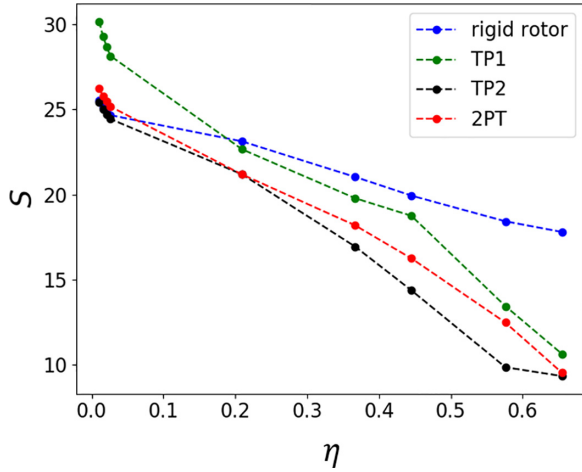


FIG. 3. Entropy of dumbbell ( $S$ ) as a function of packing fraction  $\eta$  at temperature  $T^* = 1.8$ . Here 2PT denotes entropy by use of the two-phase thermodynamic method, TP1 denotes entropy by use of thermodynamic perturbation with ideal monoatomic gas as reference and TP2 denotes entropy by use of the thermodynamic perturbation with ideal diatomic gas (rigid rotor) as reference.

The dumbbell is approximated as a rigid rotor and the entropy of the rigid rotor as a function of packing fraction is also plotted in Fig. 3. From Fig. 3 we can see that entropy from 2PT falls between entropy calculated by thermodynamic perturbation using ideal monoatomic gas (TP1) and ideal diatomic gas (TP2) as reference. Entropy from 2PT matches very closely with the entropy of rigid rotor at very low packing fraction. This small deviation is present because of the vibrational contribution of dumbbells to the entropy. The entropy from 2PT follows the entropy of rigid rotor at low packing fraction because the intermolecular interaction between dumbbells is negligible at low packing fractions but deviates from the entropy of rigid rotor as packing fraction increases. The entropy from 2PT is also close to the entropy calculated

from thermodynamic perturbation (TP2) at very low (dilute gas) and very high densities (solid). So we believe that the 2PT method can give the entropy of dumbbells very accurately.

### B. Nonequilibrium properties of equal mixture of active and passive symmetric dumbbells

Here we discuss results from simulation of equal mixture of hot and cold symmetric dumbbells. In the system of 4000 dumbbells, to bring in “activity” we introduce temperature difference between the dumbbells. Let  $T^{h*}$  and  $T^{c*}$  denote the temperatures of the “hot” and “cold” dumbbells, respectively, in reduced units. Initially, to equilibrate the system, both hot and cold dumbbells are maintained at the same temperature at  $T^{h*} = T^{c*} = 2$  and at packing fraction  $\eta = 0.42$  (equivalent to monomer number density of 0.8). The simulation in NVT ensemble is run for 4 ns so that hot and cold dumbbells mix well [Fig. 4(a)].

Initially, the temperature of the “hot” dumbbells is increased from  $T^{h*} = 2$  to  $T^{h*} = 5$  and the simulation is run for 1 ns until the system reaches a steady state. Next, the temperature of hot dumbbells is increased from  $T^{h*} = 5$  to  $T^{h*} = 10$  and eventually to  $T^{h*} = 80$  in steps of five (5, 10, 15, . . . , 80). The system is allowed to attain the steady state at each of the increased values of  $T^{h*}$  and the simulation is run for 1 ns at each temperature. After the steady state is reached, we perform a production run for  $5 \times 10^5$  time steps. The statistical averages of physical quantities were obtained by averaging over 500 configurations, sampled at a frequency of 1000 time steps in the production run. As the  $T^{h*}$  of the hot dumbbells is increased, cold dumbbells phase separate from the hot dumbbells. In Fig. 4(b), for packing fraction  $\eta = 0.42$  and  $T^{h*} = 80$ , we observe that hot and cold dumbbells are completely phase separated. As described above, simulations were also carried out at packing fraction  $\eta$  of 0.26, 0.10, and 0.05.

It is observed that even though the value of the thermostat temperature  $T^{c*}$  that is connected to the “cold” dumbbells

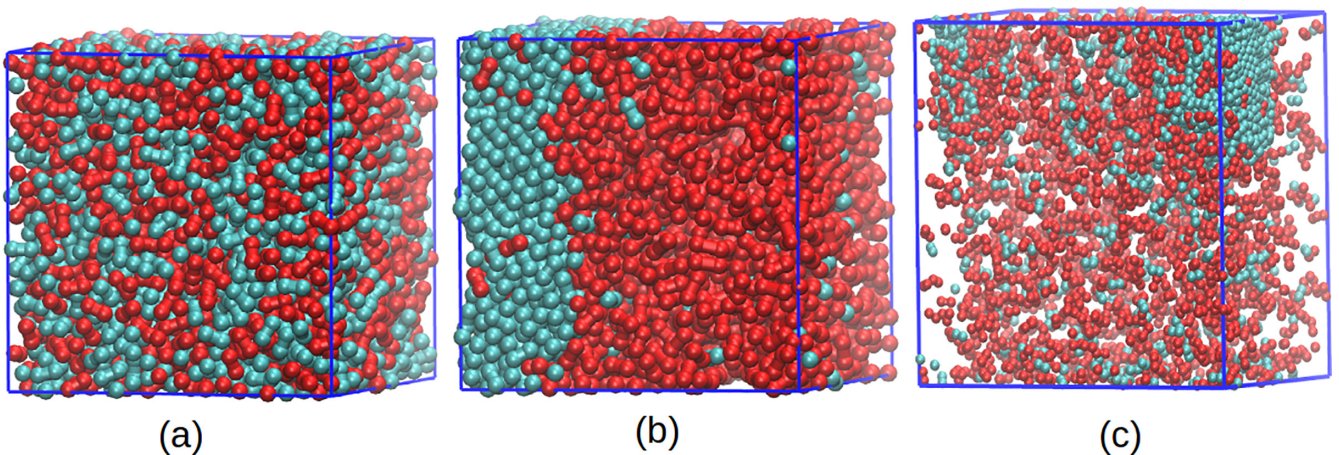


FIG. 4. (a) Instantaneous configuration of the system at the end of 4-ns-long simulation when  $T^{h*} = T^{c*} = 2$  and packing fraction  $\eta$  is 0.42. We can see that hot (red) and cold (blue) particles are well mixed. (b) Instantaneous configuration of the system at the end of 1-ns-long simulation when  $T^{h*} = 80$  and  $T^{c*} = 2$  and packing fraction  $\eta$  is 0.42. We can see that hot and cold dumbbells are clearly phase separated. (c) Instantaneous configuration of the system at the end of 1-ns-long simulation when  $T^{h*} = 80$  and  $T^{c*} = 2$  and packing fraction  $\eta$  is 0.05. Here again, hot and cold dumbbells are phase separated. The snapshots were generated using VMD [81] software.

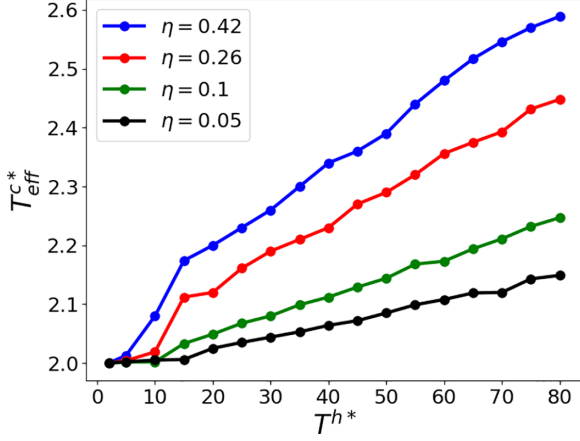


FIG. 5. Plot of effective temperature of cold dumbbells  $T_{\text{eff}}^{c*}$  versus temperature of hot dumbbells  $T^{h*}$  at different packing fractions. It is clearly seen that  $T_{\text{eff}}^{c*}$  increases with  $T^{h*}$  due to increased heat transfer from hot to cold dumbbells. Also  $T_{\text{eff}}^{c*}$  increases with packing fraction because of the increase in frequency of collisions between hot and cold dumbbells.

is left unchanged, there is an increase in the temperature of the cold dumbbells due to heat exchange from the “hot” dumbbells through interactions. Hence, they reach an “effective” temperature  $T_{\text{eff}}^{c*} > T^{c*}$ . Here the effective temperature is defined by the average kinetic energy of the dumbbells. In general,  $T^{h*} > T_{\text{eff}}^{h*} > T_{\text{eff}}^{c*} > T^{c*}$ .

The activity  $\chi$  of the system is defined as the ratio of the difference between the effective temperature of hot and cold dumbbells to the effective temperature of cold dumbbells,

$$\chi = \frac{(T_{\text{eff}}^{h*} - T_{\text{eff}}^{c*})}{T_{\text{eff}}^{c*}}. \quad (6)$$

It is the activity parameter  $\chi$  which is the measure of activity difference between hot and cold dumbbells. When both hot and cold dumbbells are at same temperature, the activity  $\chi$  is 0. As the temperature of hot dumbbells is increased, the value of  $\chi$  also increases.

The plot of effective temperature of cold dumbbells  $T_{\text{eff}}^{c*}$  versus temperature of hot dumbbells  $T^{h*}$  is shown in Fig. 5 and plot of activity  $\chi$  versus temperature of hot particles  $T^{h*}$  is given in Fig. 6.

In Fig. 5, we can see that as  $T^{h*}$  increases  $T_{\text{eff}}^{c*}$  also increases because of increased energy transfer from hot to cold dumbbells. Also, as packing fractions increase,  $T_{\text{eff}}^{c*}$  increases because with increased packing fraction, the frequency of collision between hot and cold dumbbells increases. So, the effective temperature of cold dumbbells  $T_{\text{eff}}^{c*}$  increases with the temperature of the hot subsystem and the packing fraction of the system. In Fig. 6 we can see that activity  $\chi$  increases with the temperature of hot dumbbells  $T^{h*}$  in accordance with Eq. (6). The activity  $\chi$  also decreases with packing fraction because  $T_{\text{eff}}^{c*}$  increases with the packing fraction of the system as explained before.

### 1. Order parameter

To determine the extent of phase separation, we calculate an order parameter  $\phi$ . First, divide the total volume of the

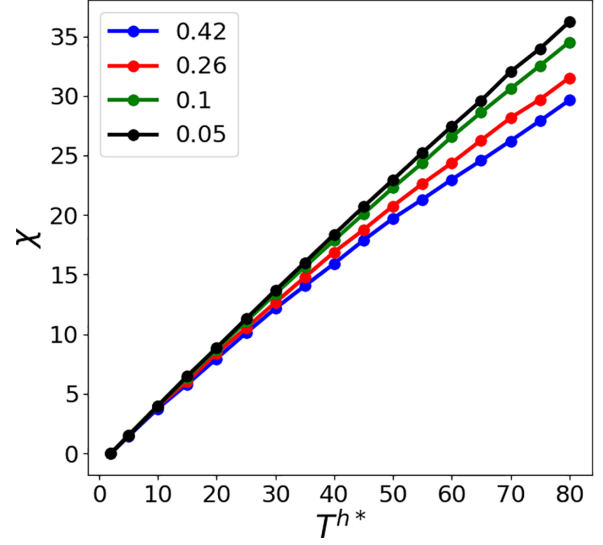


FIG. 6. Plot of activity  $\chi$  versus temperature of hot dumbbells  $T^{h*}$  at different packing fractions. In accordance with Eq. (6) activity  $\chi$  increases with increase in  $T^{h*}$ . Also  $\chi$  increases with decrease in packing fractions because  $T_{\text{eff}}^{c*}$  increases as packing fraction increases (Fig. 5).

simulation box into smaller subcells each having equal volume. Then, in each subcell, we calculate the ratio of number difference between hot and cold dumbbells to the total number of dumbbells in the subcell and average is taken over all subcells and steady configurations. The order parameter  $\phi$  is defined as follows:

$$\phi(T^{h*}) = \frac{1}{N_{\text{cell}}} \left\langle \sum_{i=1}^{N_{\text{cell}}} \frac{|n^h(i) - n^c(i)|}{[n^h(i) + n^c(i)]} \right\rangle_{\text{SS}}, \quad (7)$$

where  $n^h(i)$  and  $n^c(i)$  denote the number of hot and cold dumbbells, respectively, in the  $i$ th subcell.  $N_{\text{cell}}$  is the total number of subcells and  $\langle \rangle_{\text{SS}}$  denotes that average is taken over all steady-state configurations. In our case,  $N_{\text{cell}} = 125$ , the number is chosen such that there are enough dumbbells in each subcell.

When the value of activity  $\chi$  is low, the cold dumbbells form small clusters. As the activity is increased these small clusters join to form bigger clusters and, finally, at sufficiently high activity the phase separation becomes macroscopic where hot and cold dumbbells are clearly phase separated as shown in Fig. 4(b) and Fig. 4(c).

In Fig. 7, a plot of order parameter  $\phi$  versus activity  $\chi$  at various packing fractions is given. It can be seen that, for very small initial activity  $\chi$  the order parameter  $\phi$  remains small and constant. As  $\chi$  increases, the value of  $\phi$  also increases and finally saturates to a large value. We also find that value of  $\phi$  increases with packing fraction, indicating higher extent of phase separation at high packing fraction. Also, as packing fraction decreases, the point where  $\phi$  starts increasing is pushed to high activity. So as packing fraction decreases, the initiation of phase separation requires high activity and the extent of phase separation is also reduced.

To find out the critical activity at which macroscopic phase separation of hot and cold dumbbells take place, we plot the

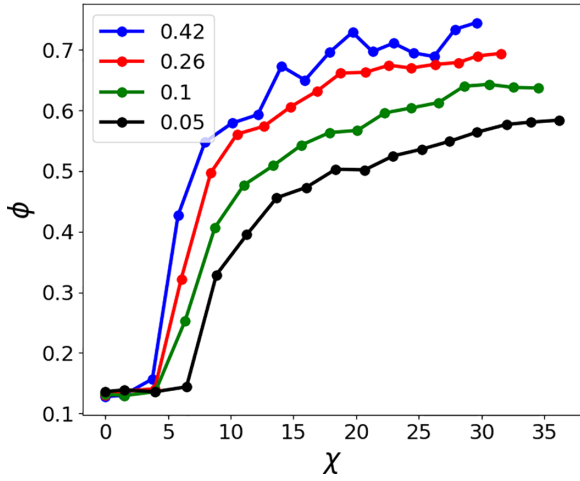


FIG. 7. Plot of order parameter  $\phi$  versus activity  $\chi$  at different packing fractions. Initially for low activity  $\chi$  order parameter  $\phi$  is small but as  $\chi$  increases  $\phi$  rises and saturates to a high value, indicating phase separation. Also the value of  $\phi$  is greater for higher packing fractions, indicating greater extent of phase separation at high packing fractions.

probability distribution of the parameter  $\psi$ . The parameter  $\psi$  in the  $i$ th subcell is defined as

$$\psi(i) = \frac{[n^h(i) - n^c(i)]}{[n^h(i) + n^c(i)]}. \quad (8)$$

The  $\psi$  takes negative values in the subcells where cold dumbbells dominate and positive values where hot dumbbells dominate. The value of  $\psi$  is close to zero when there is no phase separation and number of hot and cold dumbbells in a subcell are nearly equal. So we plot the distribution of  $\psi$  at different values of  $T^{h*}$  for each packing fraction. Figure 8 gives the distribution  $P(\psi)$  for packing fraction 0.42 and 0.05. As we increase the activity, the distribution of  $\psi$  becomes bimodal in shape when phase separation becomes macroscopic. The activity at which the distribution of  $\psi$  becomes bimodal is taken as critical activity. The bimodality in distribution of  $\psi$  occurs at  $T^{h*} = 15, 20, 20,$  and  $25$  for packing fraction  $\eta = 0.42, 0.26, 0.1,$  and  $0.05$ , respectively.

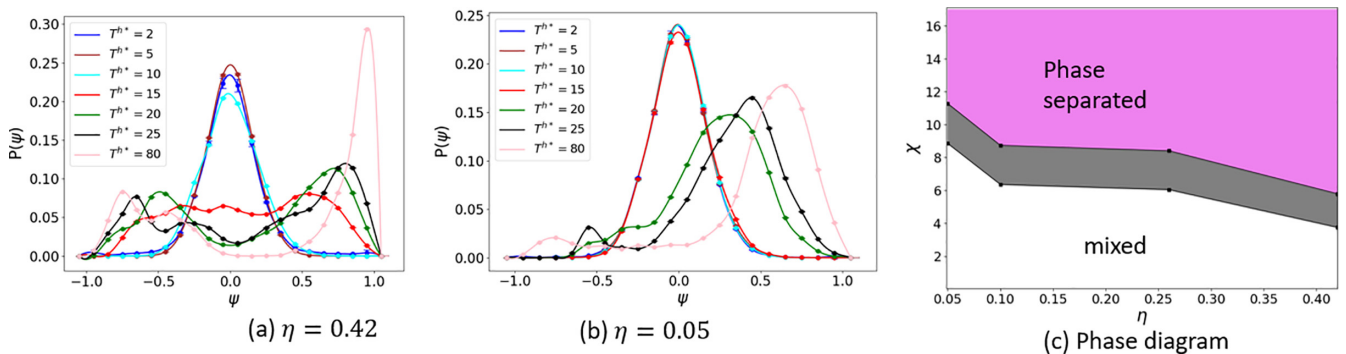


FIG. 8. [(a) and (b)] Distribution  $P(\psi)$  of parameter  $\psi$  at packing fraction 0.42 and 0.05. The bimodality in distribution  $P(\psi)$  of  $\psi$  occurs at  $T^{h*} = 15$  and  $25$  for packing fractions  $\eta = 0.42$  and  $0.05$ , respectively. These temperatures of hot dumbbells  $T^{h*}$  correspond to the critical activity of  $5.80$  and  $11.285$ . (c) Phase diagram for mixture of hot and cold dumbbells in the activity  $\chi$ -packing fraction  $\eta$  state space. The violet and white regions represent the phase-separated and mixed states of the system, respectively. The critical line of phase separation lies within the gray area.

These temperatures of hot dumbbells  $T^{h*}$  correspond to the critical activity of  $5.80, 8.41, 8.74,$  and  $11.28$ . In Fig. 8(c) we have included the phase diagram for mixture of hot and cold dumbbells in the activity  $\chi$ -packing fraction  $\eta$  state space. We can identify three regions in the phase diagram: the phase-separated region (violet), the mixed state region (white), and critical activity region (gray). The upper bound of the critical activity region corresponds to the critical activities at different packing fractions, where  $P(\psi)$  shows bimodal distribution. We also see that for activity that precedes the critical activity, the  $P(\psi)$  starts deviating from single peak distribution. We use the activity preceding critical activity at different packing fractions as lower bound for the critical activity region. Since we have simulated our system at discrete state points, we cannot precisely identify the critical activity line. The critical activity line lies inside the critical activity region we have identified in the phase diagram.

For a system of Lennard-Jones monomer [64] at packing fraction  $\eta = 0.42$ , the critical activity is  $3.44$  but at the same packing fraction for a system of dumbbells, the critical activity is  $5.80$ . So the dumbbells phase separate at a higher activity than the system of LJ monomers. These observations are in contrast to the results in Ref. [62], where authors have studied phase separation in a mixture of active and passive polymers. They have concluded that as the length of the polymer chain is increased, less activity is required for phase separation. However, they have simulated mixtures of active and passive polymers with chain-length greater than  $10$  and a very low value of spring constant for bond potential. Further study is required to know the effect of chain length and strength of bond potential on critical activity for polymers with chain length less than  $10$ . It is worth mentioning here that in a system of active and passive spherocylinders [65], as the aspect ratio of spherocylinders is increased, the critical activity of phase separation decreases.

## 2. Cluster analysis

Initially for low activity, small clusters of cold dumbbells are formed. As activity is increased, these small clusters join to form larger clusters ultimately leading to phase separation. To study the number and size of clusters, we perform cluster



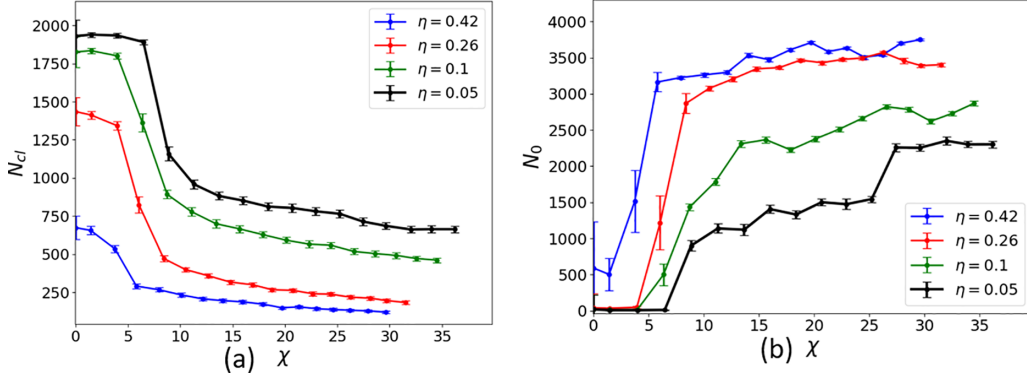


FIG. 9. (a) Number of clusters of cold dumbbells  $N_{cl}$  versus activity  $\chi$  at different packing fraction. Number of clusters of cold dumbbells  $N_{cl}$  decreases with activity  $\chi$  as small clusters join to form large clusters. (b) Plot of number of cold dumbbells in the largest cluster  $N_0$  versus activity  $\chi$  (right) at different packing fractions. Complementary to  $N_{cl}$  the number of cold dumbbells in the largest cluster  $N_0$  increases with activity  $\chi$ .

analysis. We define a cluster using the following criteria: If the distance between two atoms of different dumbbells is within a specified cut-off distance  $r_c$ , then the dumbbells are considered to be part of the same cluster. The value of the cut-off distance  $r_c$  is  $1.069\sigma$  as determined from the position of the first peak in the radial distribution function calculated between the passive-passive dumbbells as shown in Fig. 14. We plot the number of clusters of cold dumbbells  $N_{cl}$  versus activity  $\chi$  at different packing fractions in Fig. 9(a). We find that initially for small activity, when there is no phase separation, number of clusters of cold dumbbells  $N_{cl}$  is large and constant. As activity  $\chi$  is increased, phase separation sets in and the number of clusters of cold dumbbells decreases and saturates to a low value. Complementary to the number of clusters of cold dumbbells  $N_{cl}$ , the size of the largest cluster increase with activity  $\chi$  as phase separation sets in. The number of cold dumbbells  $N_0$  in the largest cluster is a measure of the size of the cluster. Plot of number of cold dumbbells in the largest cluster  $N_0$  versus activity  $\chi$  at different packing fraction is given in Fig. 9(b). Initially for low activity, when there is no phase separation, the size of largest cluster given by  $N_0$  is small and constant. As the activity  $\chi$  increases, the the size of largest cluster grows and reaches a constant value. We can see that as packing fraction increases, number of dumbbells in the largest cluster  $N_0$  also increases and hence the size of the cluster also increases, indicating higher extent phase separation.

### 3. Entropy calculation

To determine the effect of activity on hot dumbbells in nonequilibrium system with respect to their equilibrium counterparts, we calculate the entropy difference between hot dumbbells in nonequilibrium and equilibrium system. As mentioned before, in the nonequilibrium system, there is a transfer of energy from hot dumbbells to cold dumbbells due to collisions between them. Also, once the phase separation sets in, since the cold dumbbells form closely packed clusters as discussed in Section III B2, the hot dumbbells have larger effective volume. These factors affect the entropy of hot dumbbells in the nonequilibrium system. Here we have calculated the entropy per dumbbell for the hot dumbbells in

the nonequilibrium system of hot and cold dumbbells which we call  $S^{neq}$ . We compare this with the entropy per dumbbell of an equilibrium system of dumbbells (denoted as  $S^{eq}$ ) where all the dumbbells have the same temperature as that of hot dumbbells  $T^{h*}$  of the nonequilibrium system and the packing fraction of equilibrium system is taken to be equal to the average packing fraction of nonequilibrium system. We use the 2PT [83] method to calculate the entropy of hot dumbbells  $S^{neq}$  in nonequilibrium system and entropy of dumbbells in corresponding equilibrium system  $S^{eq}$ . We calculate the difference  $\Delta S$  defined as

$$\Delta S = S^{neq} - S^{eq}. \quad (9)$$

Plot of  $\Delta S$  versus  $\chi$  at various packing fractions is shown in Fig. 10. We find that initially for small activity  $\Delta S$  is negative, but as activity increases  $\Delta S$  jumps to a positive value. There are two factors which determine value of  $\Delta S$ .

1. In nonequilibrium system, there is energy transfer from hot dumbbells to cold dumbbells. It decreases the entropy of hot dumbbells  $S^{neq}$  compared to that of equilibrium system

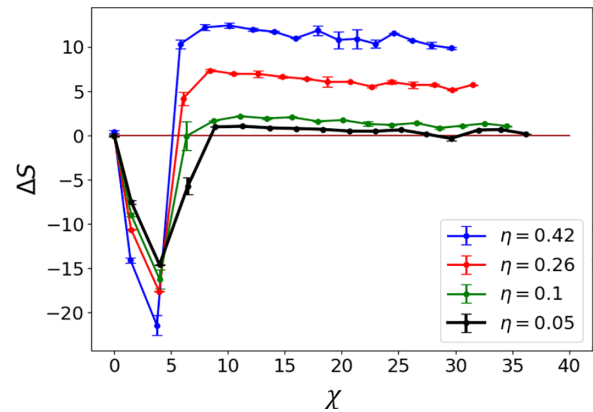


FIG. 10. Plot of entropy difference  $\Delta S = S^{neq} - S^{eq}$  versus activity  $\chi$  at different packing fractions. We can see that  $\Delta S$  is negative before the system phase separates but jumps to a positive value once the phase separation sets in. Also, we can see that the higher the packing fraction, the higher the value of  $\Delta S$ , indicating increased phase separation.

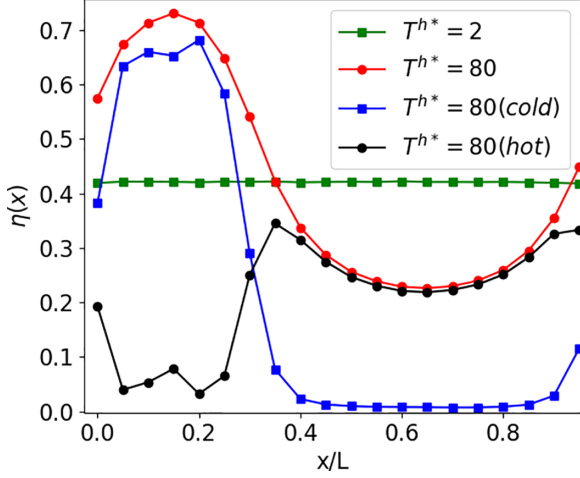


FIG. 11. Plot of packing fraction variation  $\eta(x)$  across the length of simulation box when total packing fraction  $\eta = 0.42$  at  $T^{h*} = 2$  and 80. We can see that packing fraction of cold dumbbells for  $T^{h*} = 80$  exceeds the average packing fraction 0.42 and the packing fraction of hot dumbbells decreases below average packing fraction. We can see that the interface is positioned near  $x/L \sim 0.3$ .

$S^{\text{eq}}$ . So we can see that initially for small activity where phase separation has not yet started,  $\Delta S$  is negative.

2. When there is phase separation, cold dumbbells form dense clusters and hence effective volume for hot dumbbells increases. This increase in effective volume increases  $S^{\text{neq}}$  compared to  $S^{\text{eq}}$ . As the activity is increased, phase separation takes place and  $\Delta S$  is positive.

In Fig. 10, we can also observe that the value of  $\Delta S$  increases with packing fraction hence proving that higher the packing fraction, larger is the extent of phase separation.

#### 4. Packing fraction, temperature, and pressure variation

In order to study how packing fraction and temperature varies along the length of the simulation box, the simulation box is divided in 20 subvolumes along the direction where phase separation takes place (say, the  $x$  axis). Then packing fraction in  $i$ th subvolume is given by

$$\eta(i) = \frac{n(i)v_0}{V(i)}, \quad (10)$$

where  $n(i)$  is number of dumbbells,  $V(i)$  is the volume of  $i$ th subcell and  $v_0$  is volume of individual dumbbell. Figure 11 gives the plot of packing fraction  $\eta(x)$  versus  $x/L$  for  $\eta = 0.42$  at  $T^{h*} = 2$  and  $T^{h*} = 80$ , where  $L$  is the length of simulation box along  $x$  axis. The packing fraction variation of hot and cold dumbbells has been plotted separately to find the position of interface. From the plot, the interface seems to appear somewhere near  $x/L = 0.3$ . We can see that packing fraction  $\eta(x)$  of cold dumbbells before the interface ( $x/L = 0.3$ ) is much higher than that of average packing fraction 0.42, which indicates that cold dumbbells form densely packed clusters. Also the packing fraction of hot dumbbells ( $0.4 < x/L < 0.8$ ) is much lower than that of average packing fraction 0.42.

Each atom in a dumbbell has three translational degrees of freedom. By equipartition theorem each degree of freedom contributes  $\frac{1}{2}k_bT$  of energy. Hence temperature in  $i$ th

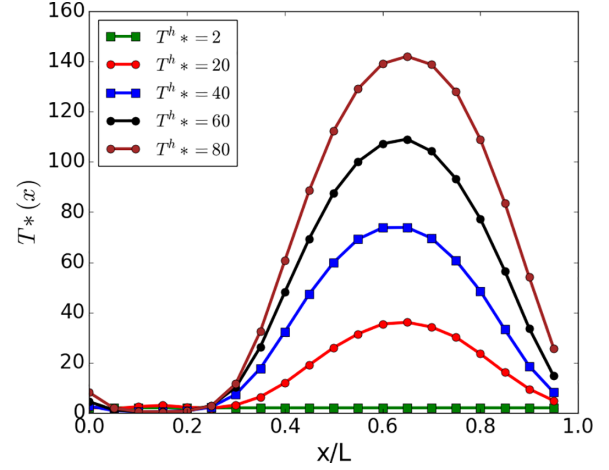


FIG. 12. Plot of temperature variation  $T^*(x)$  across the length of simulation box for  $\eta = 0.42$  at different  $T^{h*}$ . The temperature of the hot dumbbells ( $x/L > 0.4$ ) varies and decreases as we move toward the interface due to transfer of energy from hot to cold dumbbells.

subvolume is given by

$$\frac{3}{2}k_bT(i) = \frac{1}{n(i)} \sum_{j=1}^{n(i)} \frac{1}{2}mv_j^2. \quad (11)$$

Figure 12 gives plot of temperature variation of dumbbells across the interface for different values of  $T^{h*}$ . We see that temperature of hot dumbbells is not uniform but decreases as they move toward the interface, indicating energy transfer from hot to cold dumbbells. Pressure profile along the interface is calculated from diagonal components of stress tensor,

$$P(i) = \frac{1}{3 * V(i)} \left[ \sum_{j=1}^{n(i)} \frac{1}{2}mv_j^2 + \sum_{j=1}^{n(i)} \vec{r}_j \cdot \vec{f}_j \right], \quad (12)$$

$$P(i) = P_{\text{kin}}(i) + P_{\text{vir}}(i). \quad (13)$$

Here  $\vec{r}_j$  is the position vector of  $j$ th atom and  $\vec{f}_j$  is force on  $j$ th atom due to all other atoms (includes force due to interaction with other dumbbells and the force due to bonding). The first term is the kinetic part of pressure  $P_{\text{kin}}$  and second term is the virial part of pressure  $P_{\text{vir}}$ . Figure 13 gives the pressure variation across the interface when  $\eta = 0.42$  at  $T^{h*} = 80$ . We have also plotted the kinetic and virial contribution to the pressure separately. We find that the pressure is almost constant along the length of simulation box. In the regions, where the cold dumbbells dominate ( $x/L < 0.3$ ) the virial pressure  $P_{\text{vir}}$  is very high and kinetic pressure  $P_{\text{kin}}$  is low because of the low temperature of cold dumbbells. In the region where the hot dumbbells dominate ( $x/L > 0.3$ ) the kinetic pressure  $P_{\text{kin}}$  is very high because of the high temperature of hot dumbbells. So in the phase-separated system the kinetic pressure of hot dumbbells is balanced by the virial pressure of cold dumbbells.

#### 5. Bond orientation order parameter

In the previous section, from the packing fraction variation (Fig. 11), we have shown that as we increase the temperature of hot dumbbells, an initial mixed equilibrium system with



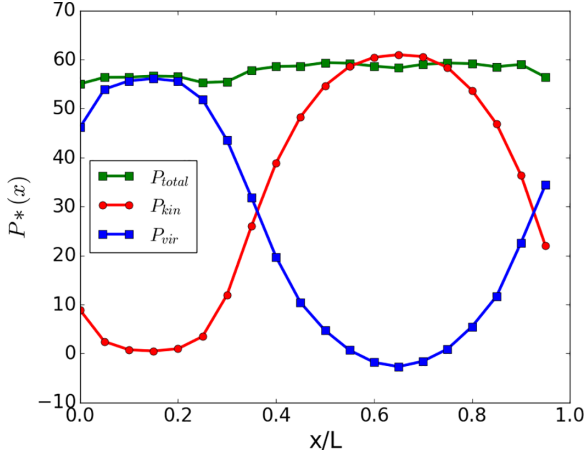


FIG. 13. Plot of pressure variation  $P^*(x)$  across the length of simulation box at density  $\eta = 0.42$  at  $T^{h*} = 80$ . The kinetic  $P_{kin}$  and virial  $P_{vir}$  contribution to the total pressure is plotted separately. The kinetic pressure of hot dumbbells is balanced by virial pressure of cold dumbbells.

uniform density, phase separates into a dense cold zone and less denser hot zone. Now to investigate the phases of hot and cold dumbbells in phase-separated system, we have calculated their radial distribution function. In Fig. 14 we have shown the radial distribution functions (RDF) of all dumbbells (blue) at  $\eta = 0.42$  and  $T^{c*} = T^{h*} = 2$  which shows liquidlike structure with damping oscillations. In Fig. 14, we have also shown RDF between cold dumbbells (black) and hot dumbbells (red) for  $\eta = 0.42$  and  $T^{h*} = 80$ . The RDF  $[g(r)]$  of cold dumbbells show crystalline order but RDF of hot dumbbells indicate a gaseous phase. So in the system of hot and cold dumbbells which is in liquid state when  $T^{c*} = T^{h*} = 2$ , as the temperature of hot dumbbells is increased, the cold dumbbells form dense clusters having crystalline order while the hot dumbbells are in gaseous phase.

In order to identify the local crystalline order, we calculate Steinhardt [86] bond order parameters. Two atoms of different

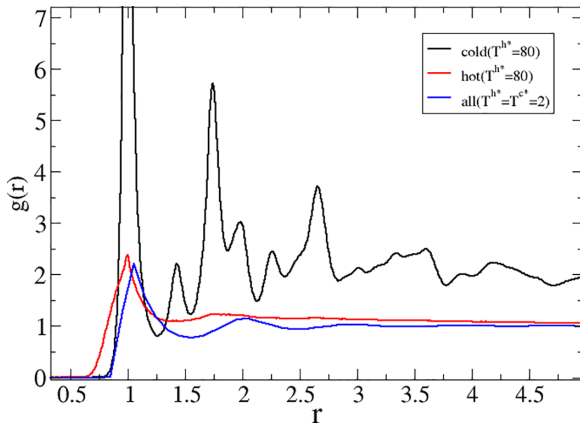


FIG. 14. The RDF  $[g(r)]$  of all dumbbells when  $T^{c*} = T^{h*} = 2$  (blue) at  $\eta = 0.42$  shows a liquidlike structure with damping oscillations. The RDF of the cold dumbbells (black) at  $\eta = 0.42$  and  $T^{h*} = 80$  indicate solidlike order but RDF of hot dumbbells (red) at  $\eta = 0.42$  and  $T^{h*} = 80$  indicate gaseous phase.

TABLE I. Value of  $q_4$  and  $q_6$  for fcc and hcp crystals.

	$q_4$	$q_6$
fcc	0.19	0.57
hcp	0.097	0.48

dumbbells are considered to be neighbors if their distance is below  $1.2\sigma$ . The bond order parameters are defined as

$$q_l(i) = \sqrt{\frac{4\pi}{2l+1} \sum_{m=-l}^l q_{lm} q_{lm}^*}, \quad (14)$$

where

$$q_{lm}(i) = \frac{1}{N_b(i)} \sum_{j=1}^{N_b(i)} Y_{lm}(\theta_{ij}, \phi_{ij}). \quad (15)$$

$N_b(i)$  corresponds to the number of bonds for particle  $i$ , and  $Y_{lm}$  is the respective spherical harmonic function. The ideal values of these parameters for various crystalline systems are given in Table I.

In Fig. 15 distribution of bond order parameters  $q_4$  and  $q_6$  when  $T^{h*} = 80$  at  $\eta = 0.42$  is given. We see that the cold dumbbells form crystalline order where the atoms of dumbbells are arranged such that they have predominantly fcc and hcp structures. Furthermore, each dumbbell points in different directions and does not possess orientational order. In an equilibrium system of dumbbells, at temperature  $T^* = 2$ , above packing fraction  $\eta = 0.567$  the dumbbells form a crystalline solid [87] where atoms of dumbbells are in fcc arrangement but the dumbbells have no orientational order and dumbbells point in different directions. In our nonequilibrium system of hot and cold dumbbells, we see that the cold dumbbells form clusters of packing fraction much greater than  $\eta = 0.567$  (Fig. 11) but the atoms of dumbbells show both hcp and fcc arrangements as evident from the calculated bond order parameters. But the cold dumbbells of the solid cluster in the nonequilibrium system also do not possess orientational order like dumbbell crystal in the equilibrium system.

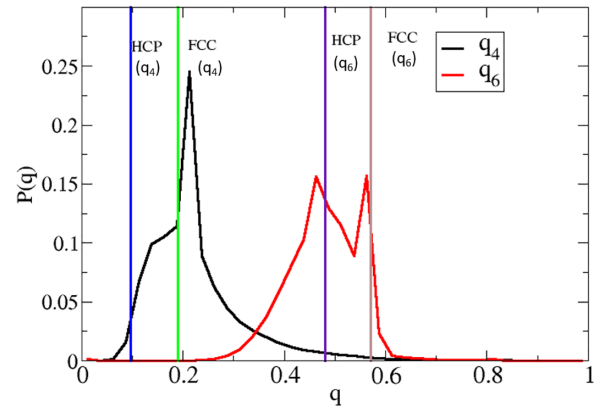


FIG. 15. Distribution of bond orientation order parameters  $q_4$  and  $q_6$  of atoms of cold dumbbells when  $T^{h*} = 80$  at  $\eta = 0.42$ . From the distribution, we can see that the cold dumbbells have predominantly fcc and hcp arrangement.

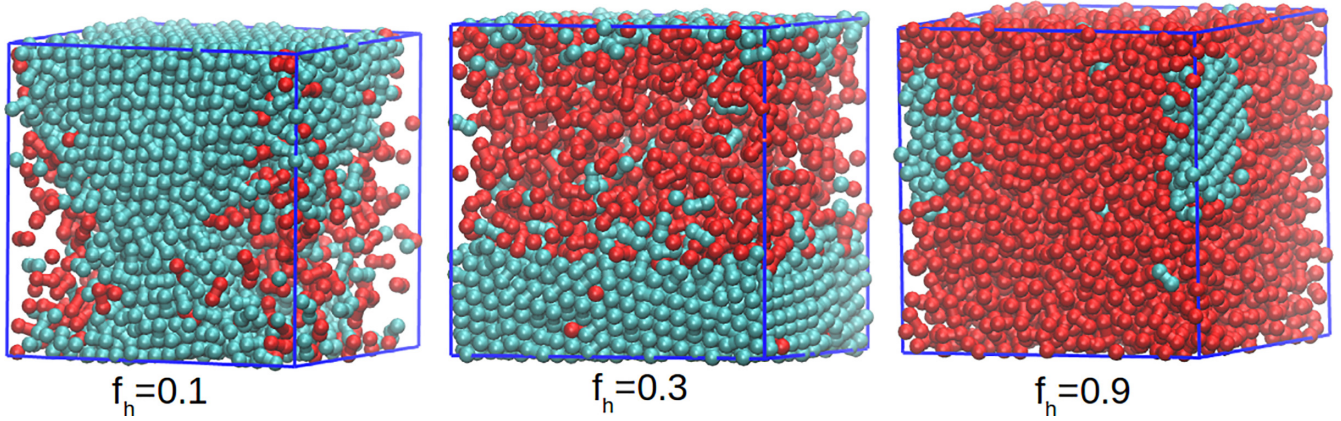


FIG. 16. Instantaneous configurations of the nonequilibrium system of hot and cold dumbbells at different fractions of hot dumbbells  $f_h$  when  $\eta = 0.42$  and  $T^{h*} = 80$ . We can see that hot and cold dumbbells phase separate at all given fractions of hot dumbbells  $f_h$ .

### C. Effect of the ratio of the number of hot and cold dumbbells on phase separation

All the results we have discussed so far correspond to 50:50 mixture of hot and cold symmetric dumbbells. We have also simulated the nonequilibrium system at different ratios of hot and cold symmetric dumbbells. The fraction of hot dumbbells  $f_h$  in the system is given by

$$f_h = \frac{\text{Number of hot dumbbells}}{\text{Total number of dumbbells}}. \quad (16)$$

Following the same procedure mentioned in Sec. III B, we have also simulated the mixture of hot and cold dumbbells for different fraction of hot dumbbells  $f_h$  0.1, 0.3, 0.7, and 0.9 at packing fraction  $\eta = 0.42$ . Figure 16 shows the instantaneous snapshots of the system at  $T^{h*} = 80$  at  $f_h$  0.1, 0.3, and 0.9. We observe that for all given fraction of hot dumbbells  $f_h$  the hot dumbbells and cold dumbbells phase separate. We plot the probability distribution  $P(\psi)$  of the parameter  $\psi$  defined in Eq. (8) for different fraction of hot dumbbells  $f_h$  to identify the critical activity at which the phase separation of hot and cold dumbbells becomes macroscopic. In Table II we give the values of critical activity for systems having different fractions of hot dumbbells  $f_h$ . From Table II we can see that as the fraction of hot dumbbells  $f_h$  increases, the value of critical activity decreases. So we can conclude that as the fraction of hot dumbbells is increased in the system, the hot and cold dumbbells start phase separating at smaller values of activity.

TABLE II. The critical activity of system of hot and cold dumbbells having different fractions of hot dumbbells  $f_h$ . We find that as the fraction of hot dumbbells  $f_h$  increases the value of critical activity decreases

$f_h$	Critical activity
0.1	15.28
0.3	8.14
0.5	5.80
0.7	3.56
0.9	3.30

### D. Effect of asymmetry of dumbbells on phase separation of hot and cold dumbbells

So far, we have discussed about nonequilibrium phase behavior of symmetric dumbbells. Here, following the same procedure described in Sec. III B, we simulated equal mixture of hot and cold asymmetric dumbbells at packing fraction  $\eta = 0.42$  with asymmetry parameter  $\alpha(\frac{\sigma_1}{\sigma_2}) = 0.2, 0.4, 0.6, 0.8,$  and 1. Figure 17 shows the snapshots of the system of asymmetric dumbbells at  $T^{h*} = 80$  with  $\alpha = 0.2, 0.4,$  and 0.8. We observe phase separation in hot and cold asymmetric dumbbells with all asymmetry parameters at high temperature of hot dumbbells.

To quantify the phase separation we have also calculated order parameter  $\phi$  defined in Eq. (7). Figure 18(a) gives the plot of order parameter  $\phi$  versus activity  $\chi$  at  $\eta = 0.42$  for asymmetric dumbbells with different asymmetry parameter  $\alpha$ . Again similar to the symmetric dumbbells, for very small initial activity  $\chi$  the order parameter  $\phi$  remains small and constant. As  $\chi$  increases, the value of  $\phi$  also increases and finally saturates to a large value, indicating phase separation. We also observe that the order parameter  $\phi$  increases with asymmetry parameter  $\alpha$  to 0.6 and does not increase further with increase in  $\alpha$ . The results for the effective temperature of cold asymmetric dumbbells and entropy of hot asymmetric dumbbells are given in Fig. 19 in the Appendix. We plot the probability distribution  $P(\psi)$  of the parameter  $\psi$  defined in Eq. (8) for dumbbells with different asymmetry parameter  $\alpha$  to identify the critical activity at which the phase separation of hot and cold dumbbells becomes macroscopic. We find that for all values of asymmetry parameter  $\alpha$ , the bimodality in distribution first occurs at  $T^{h*} = 15$  which corresponds to critical activity  $\chi \approx 5.80$ . So, the critical activity of phase separation of hot and cold asymmetric dumbbells is equal to critical activity of symmetric dumbbells irrespective of the asymmetry parameter  $\alpha$ .

The asymmetric dumbbells of asymmetry parameter  $\alpha = 0.2, 0.4, 0.6,$  and 0.8 in equilibrium [70] exist in rotator, NaCl, CrB, and  $\gamma$ CuTi crystal structures, respectively. Here we examine the arrangement of asymmetrical dumbbells in the phase-separated cold cluster. Figure 18(b) and 18(c) gives the radial distribution function  $g(r)$  of both small and large

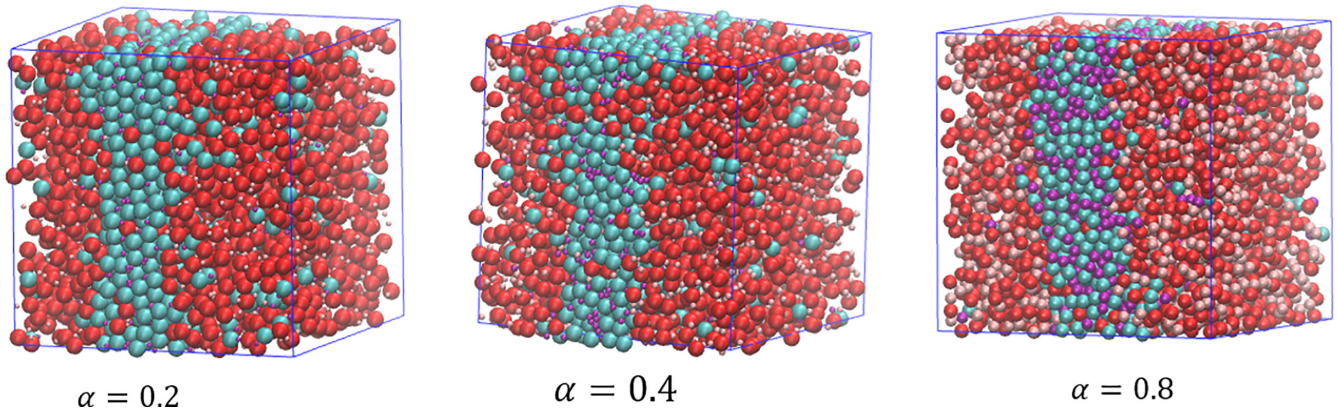


FIG. 17. Instantaneous configurations of the nonequilibrium system of hot and cold asymmetric dumbbells with different asymmetry parameters  $\alpha$  when  $\eta = 0.42$  and  $T^{h*} = 80$ . We can see that hot (pink for small atoms and red for large atoms of dumbbells) and cold (purple for small atoms and blue for large atoms of dumbbells) dumbbells phase separate for all values of asymmetry parameter  $\alpha$ .

atoms of cold dumbbells when  $T^{h*} = 80$  and  $\eta = 0.42$  for cold dumbbells with asymmetry parameter  $\alpha = 0.2$  and  $0.8$ , respectively. For asymmetric dumbbells with  $\alpha = 0.2$ , we see that the large atoms of dumbbells show crystalline order but the small atoms do not possess any crystalline order. By using bond order orientation parameters defined in Eq. (14) and (15), we find that the large atoms of dumbbells are arranged so that they have predominantly fcc and hcp structure. The small atoms of dumbbells are arranged randomly in the interstitial spaces of the large atoms of dumbbells. This structure is equivalent to the rotator crystal structure these dumbbells form under equilibrium conditions where the large atoms are in fcc arrangement and small atoms are randomly arranged in the interstitial space of large atoms. However, for dumbbells with asymmetry parameter  $\alpha = 0.4, 0.6$ , and  $0.8$ , we find that both large and small atoms of asymmetric dumbbells do not show crystalline order. This can possibly be explained from the fact that even in equilibrium [70], for  $\alpha > 0.3$  the crystal structures are not spontaneously formed upon compression of isotropic fluid because of the crystal structure being kinetically inaccessible. Since in our simulation, the cold clusters of dumbbells are formed by compression due to high kinetic

pressure of hot dumbbells, we do not observe spontaneous formation of crystal structures for  $\alpha = 0.4, 0.6$ , and  $0.8$ .

#### IV. CONCLUSION

In this work, we have extensively studied phase separation of active and passive dumbbells using two temperature scalar model of activity. In a mixture of hot and cold symmetric dumbbells, we have shown that phase separation occurs at sufficiently high temperature of hot dumbbells and the extent of phase separation increases with increase in packing fraction. We also determine the critical activity from the distribution of parameter  $\psi$  defined as the number difference between hot and cold dumbbells and find that the critical activity of dumbbells is higher than that of Lennard-Jones monomer. The critical activity also increases with decrease in packing fraction. The entropy of hot dumbbells in the nonequilibrium system increases with the activity due to increase in effective volume on phase separation. We have shown that the mechanical stability of the interface of hot and cold dumbbells is because the high kinetic pressure of hot dumbbells is balanced by the high virial pressure of cold dumbbells. We also find that

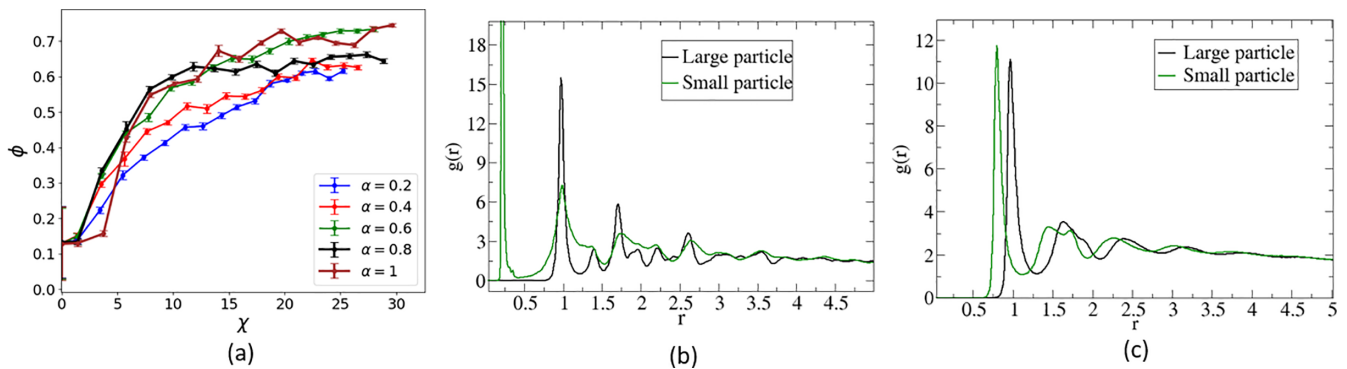


FIG. 18. (a) Plot of order parameter  $\phi$  versus activity  $\chi$  at  $\eta = 0.42$  for asymmetric dumbbells with different asymmetry parameter  $\alpha$ . Here order parameter  $\phi$  initially increases with asymmetry parameter to  $\alpha = 0.6$  but does not further increase with increase in asymmetry parameter. [(b) and (c)] The radial distribution function  $g(r)$  for both small (green) and large (black) atoms of cold dumbbells at  $T^{h*} = 80$  and  $\eta = 0.42$  for dumbbells with asymmetry parameter  $\alpha = 0.2$  and  $0.8$ , respectively. For  $\alpha = 0.2$ , the large atoms of cold dumbbells possess crystalline order but small atoms do not have crystalline ordering. For  $\alpha = 0.8$  both small and large atoms of cold dumbbells do not possess crystalline order.



critical activity decreases as we increase the fraction of hot dumbbells. We extended our simulations to study asymmetric dumbbells and find that the critical activity does not change with the asymmetry of dumbbells. The dense clusters of cold dumbbells form both crystalline and noncrystalline order depending on asymmetry parameter.

In our work without using the vectorial active force, we have shown phase separation in active and passive three-dimensional dumbbells with varied asymmetry by using two-temperature model. With the advent of artificial active systems whose persistence length can be tuned, we believe our results can be experimentally realized in mixtures of passive and driven colloidal dumbbell [77] suspensions whose persistence length is less than their size. The representation

of vectorial activity by temperature will help in developing a generalised thermodynamic approach for describing nonequilibrium active matter systems. Since dumbbells are the simplest model for anisotropic particles which are ubiquitous in nature, our simulation may help in developing theoretical frame work for scalar model of mixture of active and passive anisotropic particles.

#### ACKNOWLEDGMENTS

We thank DST, India for financial support through providing computational facility. N.V. thanks MHRD for financial assistance through scholarship.

#### APPENDIX: ADDITIONAL FIGURES

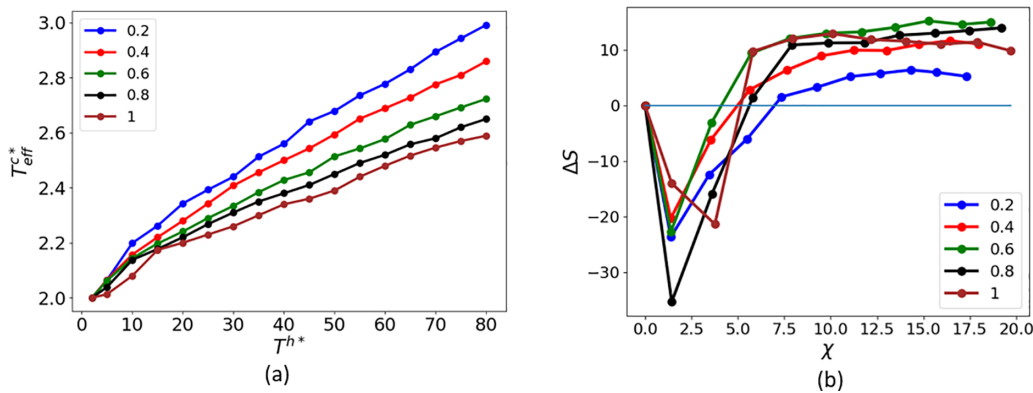


FIG. 19. (a) Plot of the effective temperature of cold dumbbells  $T_{eff}^{c*}$  versus temperature of hot dumbbells  $T^{h*}$  at  $\eta = 0.42$  for asymmetric dumbbells with different asymmetry parameter  $\alpha$ . We observe that  $T_{eff}^{c*}$  increases with decreasing asymmetry parameter  $\alpha$ . So the dumbbells with greatest asymmetry reach highest value for effective temperature of cold dumbbells  $T_{eff}^{c*}$  at a fixed packing fraction. (b) Plot of entropy difference  $\Delta S = S^{neq} - S^{eq}$  versus activity  $\chi$  at  $\eta = 0.42$  for asymmetric dumbbells with different asymmetry parameter  $\alpha$ . Here similar to the symmetric dumbbells, we observe that before phase separation entropy difference  $\Delta S$  is negative but jumps to positive value with the onset of phase separation for all values of  $\alpha$ . Also we see that entropy difference  $\Delta S$  after phase separation (positive region) increases with asymmetry parameter  $\alpha$  till 0.6 and does not increase further with increase in  $\alpha$ , following the same trend as order parameter  $\phi$  [Fig. 18(a)].

- [1] M. Gupta, B. R. Sarangi, J. Deschamps, Y. Nematbakhsh, A. Callan-Jones, F. Margadant, R.-M. Mège, C. T. Lim, R. Voituriez, and B. Ladoux, Adaptive rheology and ordering of cell cytoskeleton govern matrix rigidity sensing, *Nat. Commun.* **6**, 7525 (2015).
- [2] M. C. Marchetti, J. F. Joanny, S. Ramaswamy, T. B. Liverpool, J. Prost, M. Rao, and R. A. Simha, Hydrodynamics of soft active matter, *Rev. Mod. Phys.* **85**, 1143 (2013).
- [3] F. Jülicher, A. Ajdari, and J. Prost, Modeling molecular motors, *Rev. Mod. Phys.* **69**, 1269 (1997).
- [4] C. Bustamante, D. Keller, and G. Oster, The physics of molecular motors, *Acc. Chem. Res.* **34**, 412 (2001).
- [5] K. Kruse, J. F. Joanny, F. Jülicher, J. Prost, and K. Sekimoto, Asters, Vortices, and Rotating Spirals in Active Gels of Polar Filaments, *Phys. Rev. Lett.* **92**, 078101 (2004).
- [6] M. F. Hagan and A. Baskaran, Emergent self-organization in active materials, *Curr. Opin. Cell Biol.* **38**, 74 (2016).
- [7] A. Sokolov and I. S. Aranson, Physical Properties of Collective Motion in Suspensions of Bacteria, *Phys. Rev. Lett.* **109**, 248109 (2012).
- [8] M. M. Genkin, A. Sokolov, O. D. Lavrentovich, and I. S. Aranson, Topological Defects in a Living Nematic Ensnare Swimming Bacteria, *Phys. Rev. X* **7**, 011029 (2017).
- [9] N. Waisbord, C. T. Lefèvre, L. Bocquet, C. Ybert, and C. Cottin-Bizonne, Destabilization of a flow focused suspension of magnetotactic bacteria, *Phys. Rev. Fluids* **1**, 053203 (2016).
- [10] D. A. Matoz-Fernandez, E. Agoritsas, J.-L. Barrat, E. Bertin, and K. Martens, Nonlinear Rheology in a Model Biological Tissue, *Phys. Rev. Lett.* **118**, 158105 (2017).
- [11] J. Toner and Y. Tu, Long-range Order in a Two-Dimensional Dynamical xy Model: How Birds Fly Together, *Phys. Rev. Lett.* **75**, 4326 (1995).
- [12] J. Toner and Y. Tu, Flocks, herds, and schools: A quantitative theory of flocking, *Phys. Rev. E* **58**, 4828 (1998).

- [13] J. Tailleur and M. E. Cates, Statistical Mechanics of Interacting Run-and-Tumble Bacteria, *Phys. Rev. Lett.* **100**, 218103 (2008).
- [14] J. Toner, Y. Tu, and S. Ramaswamy, Hydrodynamics and phases of flocks, *Ann. Phys.* **318**, 170 (2005).
- [15] J. Toner, Reanalysis of the hydrodynamic theory of fluid, polar-ordered flocks, *Phys. Rev. E* **86**, 031918 (2012).
- [16] T. Vicsek, A. Czirók, E. Ben-Jacob, I. Cohen, and O. Shochet, Novel Type of Phase Transition in a System of Self-Driven Particles, *Phys. Rev. Lett.* **75**, 1226 (1995).
- [17] S. Ramaswamy, The mechanics and statistics of active matter, *Annu. Rev. Condens. Matter Phys.* **1**, 323 (2010).
- [18] P. Romanczuk, I. D. Couzin, and L. Schimansky-Geier, Collective Motion Due to Individual Escape and Pursuit Response, *Phys. Rev. Lett.* **102**, 010602 (2009).
- [19] Y.-X. Li, R. Lukeman, and L. Edelstein-Keshet, Minimal mechanisms for school formation in self-propelled particles, *Physica D* **237**, 699 (2008).
- [20] W. Yang, V. R. Misko, J. Tempere, M. Kong, and F. M. Peeters, Artificial living crystals in confined environment, *Phys. Rev. E* **95**, 062602 (2017).
- [21] I. Buttinoni, G. Volpe, F. Kümmel, G. Volpe, and C. Bechinger, Active Brownian motion tunable by light, *J. Phys.: Condens. Matter* **24**, 284129 (2012).
- [22] J. Wang and W. Gao, Nano/microscale motors: Biomedical opportunities and challenges, *ACS Nano* **6**, 5745 (2012).
- [23] G. Ozin, I. Manners, S. Fournier-Bidoz, and A. Arsenault, Dream nanomachines, *Adv. Mater.* **17**, 3011 (2005).
- [24] N. Kumar, R. K. Gupta, H. Soni, S. Ramaswamy, and A. K. Sood, Trapping and sorting active particles: Motility-induced condensation and smectic defects, *Phys. Rev. E* **99**, 032605 (2019).
- [25] F. Schmidt, B. Liebchen, H. Löwen, and G. Volpe, Light-controlled assembly of active colloidal molecules, *J. Chem. Phys.* **150**, 094905 (2019).
- [26] M. E. Cates and J. Tailleur, Motility-induced phase separation, *Annu. Rev. Condens. Matter Phys.* **6**, 219 (2015).
- [27] J. Stenhammar, R. Wittkowski, D. Marenduzzo, and M. E. Cates, Activity-Induced Phase Separation and Self-Assembly in Mixtures of Active and Passive Particles, *Phys. Rev. Lett.* **114**, 018301 (2015).
- [28] G. S. Redner, M. F. Hagan, and A. Baskaran, Structure and Dynamics of a Phase-Separating Active Colloidal Fluid, *Phys. Rev. Lett.* **110**, 055701 (2013).
- [29] I. Buttinoni, J. Bialké, F. Kümmel, H. Löwen, C. Bechinger, and T. Speck, Dynamical Clustering and Phase Separation in Suspensions of Self-Propelled Colloidal Particles, *Phys. Rev. Lett.* **110**, 238301 (2013).
- [30] S. Mandal, B. Liebchen, and H. Löwen, Motility-Induced Temperature Difference in Coexisting Phases, *Phys. Rev. Lett.* **123**, 228001 (2019).
- [31] T. Speck, J. Bialké, A. M. Menzel, and H. Löwen, Effective Cahn-Hilliard Equation for the Phase Separation of Active Brownian Particles, *Phys. Rev. Lett.* **112**, 218304 (2014).
- [32] E. Tjhung, C. Nardini, and M. E. Cates, Cluster phases and Bubbly Phase Separation in Active Fluids: Reversal of the Ostwald Process, *Phys. Rev. X* **8**, 031080 (2018).
- [33] Y. Fily, A. Baskaran, and M. F. Hagan, Dynamics of self-propelled particles under strong confinement, *Soft Matter* **10**, 5609 (2014).
- [34] H. H. Wensink, J. Dunkel, S. Heidenreich, K. Drescher, R. E. Goldstein, H. Löwen, and J. M. Yeomans, Meso-scale turbulence in living fluids, *Proc. Natl. Acad. Sci. USA* **109**, 14308 (2012).
- [35] H. R. Vutukuri, Z. Preisler, T. H. Besseling, A. van Blaaderen, M. Dijkstra, and W. T. S. Huck, Dynamic self-organization of side-propelling colloidal rods: Experiments and simulations, *Soft Matter* **12**, 9657 (2016).
- [36] S. Paliwal, J. Rodenburg, R. van Roij, and M. Dijkstra, Chemical potential in active systems: Predicting phase equilibrium from bulk equations of state? *New J. Phys.* **20**, 015003 (2018).
- [37] J. Rodenburg, M. Dijkstra, and R. van Roij, Van't hof's law for active suspensions: The role of the solvent chemical potential, *Soft Matter* **13**, 8957 (2017).
- [38] A. P. Solon, Y. Fily, A. Baskaran, M. E. Cates, Y. Kafri, M. Kardar, and J. Tailleur, Pressure is not a state function for generic active fluids, *Nat. Phys.* **11**, 673 (2015).
- [39] E. Bertin, M. Droz, and G. Grégoire, Hydrodynamic equations for self-propelled particles: Microscopic derivation and stability analysis, *J. Phys. A: Math. Theor.* **42**, 445001 (2009).
- [40] R. Mandal, P. J. Bhuyan, P. Chaudhuri, M. Rao, and C. Dasgupta, Glassy swirls of active dumbbells, *Phys. Rev. E* **96**, 042605 (2017).
- [41] R. Mandal, P. J. Bhuyan, M. Rao, and C. Dasgupta, Active fluidization in dense glassy systems, *Soft Matter* **12**, 6268 (2016).
- [42] D. Chaudhuri, Active brownian particles: Entropy production and fluctuation response, *Phys. Rev. E* **90**, 022131 (2014).
- [43] C. Ganguly and D. Chaudhuri, Stochastic thermodynamics of active Brownian particles, *Phys. Rev. E* **88**, 032102 (2013).
- [44] S. Chakraborty and S. K. Das, Relaxation in a phase-separating two-dimensional active matter system with alignment interaction, *J. Chem. Phys.* **153**, 044905 (2020).
- [45] B. Bhattacharjee and D. Chaudhuri, Re-entrant phase separation in nematically aligning active polar particles, *Soft Matter* **15**, 8483 (2019).
- [46] S. Chaki and R. Chakrabarti, Escape of a passive particle from an activity-induced energy landscape: Emergence of slow and fast effective diffusion, *Soft Matter* **16**, 7103 (2020).
- [47] R. Netz, Fluctuation-dissipation relation and stationary distribution of an exactly solvable many-particle model for active biomatter far from equilibrium, *J. Chem. Phys.* **148**, 185101 (2018).
- [48] L. Caprini and U. Marini Bettolo Marconi, Spatial velocity correlations in inertial systems of active brownian particles, *Soft Matter* **17**, 4109 (2021).
- [49] L. Caprini, U. Marini Bettolo Marconi, and A. Puglisi, Spontaneous Velocity Alignment in Motility-Induced Phase Separation, *Phys. Rev. Lett.* **124**, 078001 (2020).
- [50] Z. Ma, Q.-I. Lei, and R. Ni, Driving dynamic colloidal assembly using eccentric self-propelled colloids, *Soft Matter* **13**, 8940 (2017).
- [51] J. Stenhammar, D. Marenduzzo, R. J. Allen, and M. E. Cates, Phase behaviour of active brownian particles: The role of dimensionality, *Soft Matter* **10**, 1489 (2014).
- [52] S. Hermann, P. Krinninger, D. de las Heras, and M. Schmidt, Phase coexistence of active brownian particles, *Phys. Rev. E* **100**, 052604 (2019).
- [53] R. W. Nash, R. Adhikari, J. Tailleur, and M. E. Cates, Run-and-Tumble Particles with Hydrodynamics: Sedimenta-

- tion, Trapping, and Upstream Swimming, *Phys. Rev. Lett.* **104**, 258101 (2010).
- [54] B. Ezhilan, R. Alonso-Matilla, and D. Saintillan, On the distribution and swim pressure of run-and-tumble particles in confinement, *J. Fluid Mech.* **781**, R4 (2015).
- [55] H. Tanaka, A. A. Lee, and M. P. Brenner, Hot particles attract in a cold bath, *Phys. Rev. Fluids* **2**, 043103 (2017).
- [56] A. Suma, G. Gonnella, G. Laghezza, A. Lamura, A. Mossa, and L. F. Cugliandolo, Dynamics of a homogeneous active dumbbell system, *Phys. Rev. E* **90**, 052130 (2014).
- [57] E. Ben-Isaac, Y. K. Park, G. Popescu, F. L. H. Brown, N. S. Gov, and Y. Shokef, Effective Temperature of Red-Blood-Cell Membrane Fluctuations, *Phys. Rev. Lett.* **106**, 238103 (2011).
- [58] X.-L. Wu and A. Libchaber, Particle Diffusion in a Quasi-Two-Dimensional Bacterial Bath, *Phys. Rev. Lett.* **84**, 3017 (2000).
- [59] A. Y. Grosberg and J.-F. Joanny, Nonequilibrium statistical mechanics of mixtures of particles in contact with different thermostats, *Phys. Rev. E* **92**, 032118 (2015).
- [60] R. R. Netz, Approach to equilibrium and nonequilibrium stationary distributions of interacting many-particle systems that are coupled to different heat baths, *Phys. Rev. E* **101**, 022120 (2020).
- [61] S. N. Weber, C. A. Weber, and E. Frey, Binary Mixtures of Particles with Different Diffusivities Demix, *Phys. Rev. Lett.* **116**, 058301 (2016).
- [62] J. Smrek and K. Kremer, Small Activity Differences Drive Phase Separation in Active-Passive Polymer Mixtures, *Phys. Rev. Lett.* **118**, 098002 (2017).
- [63] N. Ganai, S. Sengupta, and G. I. Menon, Chromosome positioning from activity-based segregation, *Nucleic Acids Res.* **42**, 4145 (2014).
- [64] S. S. N. Chari, C. Dasgupta, and P. K. Maiti, Scalar activity induced phase separation and liquid-solid transition in a Lennard-Jones system, *Soft Matter* **15**, 7275 (2019).
- [65] J. Chattopadhyay, S. S. P. Sivajothi, K. Varma, S. Ramaswamy, C. Dasgupta, and P. K. Maiti, Heating leads to liquid-crystal and crystalline order in a two-temperature active fluid of rods, *Phys. Rev. E* **104**, 054610 (2021).
- [66] J. Chattopadhyay, S. Ramaswamy, C. Dasgupta, and P. K. Maiti, Two-temperature activity induces liquid-crystal phases inaccessible in equilibrium, *Phys. Rev. E* **107**, 024701 (2023).
- [67] D. Rajendra, J. Mandal, Y. Hatwalne, and P. K. Maiti, Packing and emergence of the ordering of rods in a spherical monolayer, *Soft Matter* **19**, 137 (2022).
- [68] C. Vega, C. McBride, E. de Miguel, F. J. Blas, and A. Galindo, The phase diagram of the two center Lennard-Jones model as obtained from computer simulation and Wertheim's thermodynamic perturbation theory, *J. Chem. Phys.* **118**, 10696 (2003).
- [69] C. Vega and P. A. Monson, Solid-fluid equilibria for quadrupolar hard dumbbells via monte carlo simulation, *J. Chem. Phys.* **102**, 1361 (1995).
- [70] M. Dennison, K. Milinković, and M. Dijkstra, Phase diagram of hard snowman-shaped particles, *J. Chem. Phys.* **137**, 044507 (2012).
- [71] A. Šarić, B. Bozorgui, and A. Cacciuto, Packing of soft asymmetric dumbbells, *J. Phys. Chem. B* **115**, 7182 (2011).
- [72] J. D. Forster, J.-G. Park, M. Mittal, H. Noh, C. F. Schreck, C. S. O'Hern, H. Cao, E. M. Furst, and E. R. Dufresne, Assembly of optical-scale dumbbells into dense photonic crystals, *ACS Nano* **5**, 6695 (2011).
- [73] D. Zerrouki, J. Baudry, D. Pine, P. Chaikin, and J. Bibette, Chiral colloidal clusters, *Nature (Lond.)* **455**, 380 (2008).
- [74] K. Milinković, M. Dennison, and M. Dijkstra, Phase diagram of hard asymmetric dumbbell particles, *Phys. Rev. E* **87**, 032128 (2013).
- [75] A. Suma, G. Gonnella, D. Marenduzzo, and E. Orlandini, Motility-induced phase separation in an active dumbbell fluid, *Europhys. Lett.* **108**, 56004 (2014).
- [76] L. F. Cugliandolo, P. Digregorio, G. Gonnella, and A. Suma, Phase Coexistence in Two-Dimensional Passive and Active Dumbbell Systems, *Phys. Rev. Lett.* **119**, 268002 (2017).
- [77] M. Y. Ben Zion, Y. Caba, A. Modin, and P. M. Chaikin, Cooperation in a fluid swarm of fuel-free micro-swimmers, *Nat. Commun.* **13**, 184 (2022).
- [78] J. K. Johnson, E. A. Mueller, and K. E. Gubbins, Equation of state for lennard-jones chains, *J. Phys. Chem.* **98**, 6413 (1994).
- [79] S. Plimpton, Fast parallel algorithms for short-range molecular dynamics, *J. Comput. Phys.* **117**, 1 (1995).
- [80] T. Goel, C. N. Patra, T. Mukherjee, and C. Chakravarty, Excess entropy scaling of transport properties of Lennard-Jones chains, *J. Chem. Phys.* **129**, 164904 (2008).
- [81] W. Humphrey, A. Dalke, and K. Schulten, VMD—Visual molecular dynamics, *J. Mol. Graph.* **14**, 33 (1996).
- [82] J. K. Johnson, J. A. Zollweg, and K. E. Gubbins, The Lennard-Jones equation of state revisited, *Mol. Phys.* **78**, 591 (1993).
- [83] S.-T. Lin, M. Blanco, and W. A. Goddard, The two-phase model for calculating thermodynamic properties of liquids from molecular dynamics: Validation for the phase diagram of Lennard-Jones fluids, *J. Chem. Phys.* **119**, 11792 (2003).
- [84] S.-T. Lin, P. K. Maiti, and W. A. Goddard, Two-phase thermodynamic model for efficient and accurate absolute entropy of water from molecular dynamics simulations, *J. Phys. Chem. B* **114**, 8191 (2010).
- [85] T. A. Pascal, S.-T. Lin, and W. A. Goddard III, Thermodynamics of liquids: Standard molar entropies and heat capacities of common solvents from 2pt molecular dynamics, *Phys. Chem. Chem. Phys.* **13**, 169 (2011).
- [86] P. J. Steinhardt, D. R. Nelson, and M. Ronchetti, Bond-orientational order in liquids and glasses, *Phys. Rev. B* **28**, 784 (1983).
- [87] C. Vega, F. J. Blas, and A. Galindo, Extending wertheim's perturbation theory to the solid phase of Lennard-Jones chains: Determination of the global phase diagram, *J. Chem. Phys.* **116**, 7645 (2002).